W. M. Keck Institute for Space Studies
Final Report

Erik Shirokoff
August 2011 - May 2013

In the history of the universe, much of the radiation emitted from the UV to the near-IR by stars and black holes has been obscured by the dust in the local environment and re-radiated in the far-infra red (far-IR). The integrated intensity of this cosmic far-IR background is comparable to the optical / near-IR [1], indicating that obscured star formation and black hole growth are important in understanding the history of galaxies responsible for the first generations of stars and the reionization of the intergalactic medium (the transition of the intergalactic medium from neutral to ionized hydrogen at a redshift of $z \geq 6$).

Large far-IR, submm, and mm-wavelength imaging surveys, most recently Herschel and the South Pole Telescope (SPT), are now revealing the sources that created this background. The Herschel maps are confusion limited, but reveal hundreds to thousands of bright sources per square degree. Most are at redshift 1–3, but selection based on the far-IR colors can be used to identify potential high-redshift sources as high as $z > 6$ [2, 3]. The very brightest are gravitationally lensed, presenting an opportunity to study typical galaxies in the early Universe which would normally be undetectable [4, 5, 6]. Ground-based surveys at longer wavelengths such as those of the SPT [7] and SCUBA-2 / JCMT [8]will produce $\sim 10^6$ dusty galaxies from which interesting sub-samples could be identified for detailed study. After two years of observations with the future Cerro Chajnantor Atacama Telescope (CCAT) 40-kilopixel first-light camera, this sample could grow by two orders of magnitude.

Spectroscopy of these sources remains a bottleneck. Many do not have unambiguously-identifiable optical / near-IR counterparts due to high dust extinction.[9]. For the lensed sources, optical/near-IR counterparts are often weaker than and confused with the lens. Where counterparts exist, such measurements provide little information about the embedded energy sources [10]. The most reliable and direct way to find redshifts and study conditions in these galaxies is with their far-IR/submm spectra.The rotational lines of CO combined with the suite of far-IR fine-structure lines provide an unambiguous redshift template, with good sensitivity to high redshifts via the 158 µm [CII] transition in the 1-mm window. The line fluxes also provide unique and quantitative astrophysical information as they are not subject to dust extinction.

A large, wide-field submm telescope equipped with a wide-band multi-object spectroscopic capability will be necessary to obtain redshifts and spectra for a cosmologically-interesting sample of these high-redshift dusty sources. In order to build such an instrument – as well as future space-based instruments at shorter wavelengths where atmospheric absorption makes ground based instruments impractical – we must develop new technologies that enable inexpensive spectrometers that are compact, densely-multiplexed, and background-limited.

The SuperSpec technology and readout infrastructure which I've worked to develop during my KISS postdoctoral fellowship will, in the next few years, enable the construction of a ∼100-pixel Multi Object Spectrometer (MOS) for a large submm telescope. In particular, our collaboration has proposed an instrument for CCAT, called X-Spec, that employs several hundred horn-coupled spectrometers and a steerable optical feed to track individual sources. The same instrument, or a similar device with simpler fixed optics, could be used to measure the tomographic signature (e.g., 3-D equivalent of a power spectrum) of the emission from the unresolved galaxies responsible for reionization. Future generations of a SuperSpec-based spectrometer could field $\geq 10^3$ focal-plane pixels, allowing for integral field unit instruments able to map the sky for discrete sources without a need for a steered feed.

SuperSpec is an ultra-compact, wide-band spectrometer-on-a-chip for mm and submm wavelength astronomy. The kinetic inductance detector (KID)-based design we've been pursuing is similar to other filter-bank spectrometers which appear in the literature, [11, 12, 13] and the contemporary project DESHIMA.[14, 15] The Tomographic Ionized-Carbon Mapping Experiment (TIME) project (described below) is testing devices which use a similar microstrip filter bank coupled to Transition Edge Sensor (TES) bolometers.

In this design, mm-wave radiation incident on an antenna or feedhorn propagates along a transmission line (the feedline) and past a series of half-wavelength transmission line mm-wave resonators. Each resonator is weakly coupled both to the feedline and to a power-detector, and thus functions as a tuned filter. The resonator frequencies are arranged monotonically and physically spaced quarter-wavelength from neighboring channels to minimize interaction between resonators. Each mm-wave resonator is coupled to a kinetic inductance detector (KID). These devices rely on thin-film, high quality factor (Q) microresonators that change resonant frequency in response to absorbed radiation. These changes may be monitored by recording the complex transmission of an RF or microwave tone tuned to the resonant frequency. The response is linear provided changes in the loading are small. Due to the high quality factors (narrow linewidths) that can be achieved, thousands of KIDs may be read out on a single RF/microwave feed line, using no cryogenic electronics except a single cold (4–20 K) microwave amplifier.

KID technology is now approaching the performance levels of the SQUID-multiplexed bolometer systems in multiple ground-based cameras worldwide (e.g. MUSIC [16] and NIKA [17, 18]) and has accelerated in new directions with the Caltech / JPL discovery of the outstanding properties of the superconducting nitride materials, in particular TiN [19]. TiN has a high normal state impedance, important for achieving low readout frequencies, but most interesting is the very high Q values (3×10^7) achieved with TiN resonators. These high Qs, along with the other properties of TiN make it possible to build sensitive devices, and dark NEPs as low as $4 \times 10^{-19}\,\mathrm{W\,Hz^{-1/2}}$ have been measured by members of our group.

During my KISS postdoctoral fellowship, I've principally worked on the design and testing of two generations of prototype SuperSpec spectrometers, in collaboration with a team of researchers at Caltech and JPL lead by Matt Bradford and Jonas Zmuidzinas. We've assembled a telescope-ready optical cryostat and test bed, designed and tested two generations of optical test devices, and refined the laboratory techniques required to characterize hundreds of narrow band spectrometer KIDs. In addition to the three conference proceedings included here, additional discussion of the SuperSpec technology can be found in references [20] and [21].

The SuperSpec collaboration has demonstrated a number of key technologies required for an astronomically viable spectrometer: (1) measured mm-wave channel profiles that show detailed electromagnetic coupling in close agreement with simulations for multi-channel resonator circuits (2) rejection of directly-absorbed out-of-band power at better than 10^{-3} for narrow spectral channels (3) total dieletric losses corresponding to a limiting resonator Q of ~ 1400, suitable for an astronomically viable instrument (4) inferred Noise Equivalent Power (NEP) referenced at the detector of $3 \times 10^{-16}\,\mathrm{WHz^{-1/2}}$ (5) optical coupling using both a custom smooth-walled wide-band feedhorn and probe design and a narrow-band but easily fabricated design using a twin-slot antenna and a silicon hyper-hemispherical lens.

There remain two significant goals which are must be met in order to field a scientifically viable demonstration instrument: (1) Our NEP is a factor of 2-6 higher than the background limit for proposed science applications, due primarily to the lower than expected measured responsivity of our devices. We are currently engaged in both tests designed to carefully measure the relationship between response and loading in our TiN films, and in the design of a new generation of devices which should approach the photon noise limit given our measured film properties. (2) The center frequencies of our mm-wave channels show a random scatter which is significantly larger than can be explained using electromagnetic simulations and conservative estimates of the variation of material properties. A new prototype design including lithographically-adjustable resonators arranged in filter banks with identical dimensions will explore this variation, and designs incorporating alternative dielectrics (amorphous Si; crystal Si in a SOI device layer) are underway. The collaboration expects to achieve both of these goals within the next year or two, and has applied for external funding to continue this research, with the goal of fabricating and deploying a demonstration instrument in 2016. I will continue to lead the detector design program in my new position at the University of Chicago, in close collaboration with the Caltech team and the JPL MDL.

In addition to the the work on SuperSpec, I've participated in two other scientific programs. The first is the TIME and TIME-*Pilot* collaboration. This project, supported in part by a KISS technical development program and lead by Jamie Bock at Caltech, will develop an instrument that can measure the tomographic signature of ionized carbon [CII] emission from the high redshift galaxies responsible for reionization. In addition to the testing of a bolometer-based channelizer spectrometer similar to the SuperSpec design, the collaboration intends to field a grating spectrometer within two years, using repurposed hardware and grating and detector technology based upon the successful *Z-Spec* and *BICEP-II / KECK Array* CMB instruments.

I've also remained a part of collaboration associated with my thesis work, SPT. I've participated in collaboration meetings and contributed to the working group analyzing the Cosmic Microwave Background and secondary-anisotropy power spectrum from the complete 2500 square degree SPT survey and the cross correlation of SPT data with Herschel/SPIRE data which we expect to publish in the next year.

Finally, while a KISS fellow I chaired the Local Organizing Committee for the 15th Annual workshop on Low Temperature Detectors (LTD-15), which was hosted by Caltech and held at the Pasadena Convention Center in June 2013. This bienniel week-long conference focused on the development of cryogenic detectors for a range of scientific applications drew 342 participants from institutions in 15 countries. As LOC chair, I also served as guest editor for the peer-reviewed proceedings which will appear as a series of special issues of the Journal of Low Temperature Physics from Aug-Nov 2014.

Acknowledgments

I would like to thank the W. M. Keck Institute for Space Studies for their support of the research discussed here. In addition to my postdoctoral fellowship, I've benefited from participating in two workshops and technical development programs: the *Superconducting Nitride Detector Workshop* and the *Intensity Mapping of Carbon Monoxide from the Epoch of Reionization* technical development program. I am also grateful to the Caltech KIDs group, the Caltech Observational Cosmology group, and the CCAT collaboration for the shared resources and fruitful discussions they've provided. I would also like to personally thank Michele Judd and Tom Prince at KISS, my postdoctoral advisor Jonas Zmuidzinas, and the SuperSpec PI Matt Bradford, for their support and guidance.

The SuperSpec Project received additional support from the NASA Astrophysics Research and Analysis (APRA) grant no. 399131.02.06.03.43. Co-authors Chris M. McKenney, and Loren J. Swenson also acknowledge support from KISS. Co-authors Matt I. Hollister, Loren J. Swenson, and Theodore Reck acknowledge support from the NASA Postdoctoral Program. Peter S. Barry acknowledges the continuing support from the Science and Technology Facilities Council Ph.D studentship programme and grant programmes ST/G002711/1 and ST/J001449/1. Device fabrication was performed the JPL Microdevices Laboratory.

References

[1] D. J. Fixsen, C. L. Bennett, and J. C. Mather, *ApJ* **526**, 207 (1999).

[2] C. D. Dowell et al., *ArXiv e-prints* (2013).

[3] D. A. Riechers et al., *Nature* **496**, 329 (2013).

[4] M. Negrello et al., *Science* **330**, 800 (2010).

[5] R. E. Lupu et al., *ApJ* **757**, 135 (2012).

[6] K. S. Scott et al., *ApJ* **733**, 29 (2011).

[7] J. D. Vieira et al., *ApJ* **719**, 763 (2010).

[8] J. E. Geach et al., *MNRAS* **432**, 53 (2013).

[9] K. Menéndez-Delmestre et al., *ApJ* **699**, 667 (2009).

[10] A. M. Swinbank et al., *MNRAS* **405**, 234 (2010).

[11] J. A. Tauber and N. R. Erickson, *Rev. of Sci. Inst.* **62**, 1288 (1991).

[12] C. J. Galbraith et al., *IEEE Trans. circuits and systems I* **55**, 969 (2008).

[13] C. J. Galbraith, Ph.D. thesis, U. Michigan (2008).

[14] A. Endo et al., *J. Low Temp. Phys.* **167**, 341 (2012).

[15] A. Endo et al., *Appl. Phys. Lett.* **103**, 032601 (2013).

[16] J. A. Schlaerth et al., vol. 7741 of *Proceedings of SPIE*, 77410F (2010).

[17] A. Monfardini et al., *ApJS* **194**, 24 (2011).

[18] R. Adam et al., *ArXiv e-prints* (2013).

[19] H. G. Leduc et al., *Appl. Phys. L.* **97** (2010).

[20] A. Kovács et al., *Proc. SPIE* **8452**, 84522G (2012).

[21] P. S. Barry et al., *Proc. SPIE* **8452**, 84522F (2012).

MKID development for SuperSpec: an on-chip, mm-wave, filter-bank spectrometer

E. Shirokoff[a], P. S. Barry[b], C. M. Bradford[c], G. Chattopadhyay[c], P. Day[c], S. Doyle[b], S. Hailey-Dunsheath[a], M. I. Hollister[a,c], A. Kovács[a,d], C. McKenney[a], H. G. Leduc[c], N. Llombart[e], D. P. Marrone[f], P. Mauskopf[b,g], R. O'Brient[a,c], S. Padin[a], T. Reck[c], L. J. Swenson[a,c], J. Zmuidzinas[a,c]

[a]California Institute of Technology, Pasadena, CA, U.S.A.
[b]School of Physics & Astronomy, Cardiff University, Cardiff, Wales, U.K.
[c]Jet Propulsion Laboratory, Pasadena, CA, U.S.A.
[d]Univ. of Minnesota, Twin Cities, MN, U.S.A.
[e]Complutense University of Madrid, Spain;
[f]Steward Observatory & University of Arizona, Tucson, AZ, U.S.A;
[g]Arizona State University, Tempe, AZ, U.S.A.

ABSTRACT

SuperSpec is an ultra-compact spectrometer-on-a-chip for millimeter and submillimeter wavelength astronomy. Its very small size, wide spectral bandwidth, and highly multiplexed readout will enable construction of powerful multibeam spectrometers for high-redshift observations. The spectrometer consists of a horn-coupled microstrip feedline, a bank of narrow-band superconducting resonator filters that provide spectral selectivity, and kinetic inductance detectors (KIDs) that detect the power admitted by each filter resonator. The design is realized using thin-film lithographic structures on a silicon wafer. The mm-wave microstrip feedline and spectral filters of the first prototype are designed to operate in the band from 195-310 GHz and are fabricated from niobium with at T_c of $9.2\,K$. The KIDs are designed to operate at hundreds of MHz and are fabricated from titanium nitride with a T_c of $\sim 2\,$K. Radiation incident on the horn travels along the mm-wave microstrip, passes through the frequency-selective filter, and is finally absorbed by the corresponding KID where it causes a measurable shift in the resonant frequency. In this proceedings, we present the design of the KIDs employed in SuperSpec and the results of initial laboratory testing of a prototype device. We will also briefly describe the ongoing development of a demonstration instrument that will consist of two 500-channel, R=700 spectrometers, one operating in the 1-mm atmospheric window and the other covering the 650 and 850 micron bands.

Keywords: kinetic inductance detector, MKID, resonator, titanium nitride, mm-wavelength, spectroscopy

1. INTRODUCTION

The epoch of reionization, and the birth and subsequent growth of galaxies and clusters in the first half of the Universe's history are key topics in modern astrophysics. At present, the bulk of our information about this important epoch comes from studies in the rest-frame ultraviolet. Yet measurement of the cosmic far-IR background indicates that in aggregate, half the energy released by stars, star formation, and accretion through the Universe's history has been absorbed and reradiated by dust and gas at mm and submm wavelengths.

Spectroscopic surveys at millimeter wavelengths, using a multi-pixel spectrometer such as we describe here on a large telescope, are uniquely poised to access the high-redshift Universe, both through the measurement of individual galaxies, and via statistical studies in wide-field tomography. In particular, the 157.7μm [CII] transition is typically the brightest spectral feature in dusty galaxies. It carries $\sim 0.1\%$ of the total luminosity, and promises to be a powerful probe of galaxies beyond redshift 3.0 where it is redshifted into the atmospheric transmission windows at wavelengths $\geq 600\,\mu$m.

Direct correspondence to E. Shirokoff: erik.shirokoff@caltech.edu

[CII] spectroscopy, combined with dust continuum measurements, allows for the determination of temperature and luminosity, and provides a direct and unbiased measure of the galaxy luminosity function and the history of star formation. Additional science targets include the evolution of atomic and molecular gas properties via [CII] and CO line surveys of optical catalog targets, and the unique ability to measure galaxy clustering and the galaxy power spectrum ($P(k)$) at high redshifts ($z > 4$).

SuperSpec is a novel, ultra-compact spectrometer-on-a-chip for millimeter and submillimeter wavelength astronomy. Its very small size, wide spectral bandwidth, and highly multiplexed detector readout will enable construction of powerful multibeam spectrometers for high-redshift observations. This filter-bank spectrometer employs high-density, planar, lithographic fabrication techniques, and easily fabricated and naturally multiplexed KIDs.

During the next year, we will build a demonstration instrument using the SuperSpec technology. This camera will include at least two spectrometer pixels, one in the 195-310 GHz atmospheric band, and one in the 320-520 GHz band, each with 600 channels with a resolution of $\mathcal{R} = 700$. We then aim to apply this technology to a proposed direct-detection wide-band survey spectrometer for the Cerro Chajnantor Atacama Telescope (CCAT) with tens to hundreds of pixels. The proposed instrument, nominally called *X-Spec* will be optimized for measuring the bright atomic fine-structure and molecular rotational transitions from interstellar gas in galaxies. A 300-pixel, dual-band spectrometer based on this technology would be more than an order of magnitude faster than ALMA for full-band extra-galactic surveys.

2. MM-WAVELENGTH CIRCUIT

The KID-based design outlined here is a specific example of the filter-bank spectrometer circuit discussed in more detail in Kovács et. al.[1] The basic design is similar to other filter-bank spectrometers which appear in the literature,[2–4] as well as the contemporary project DESHIMA.[5] In this design, incoming radiation propagates down a transmission line (the feedline) and past a series of N_c tuned resonant filters. Each filter consists of a section of transmission line with a length of $\lambda_i/2$ where λ_i is the propagation wavelength corresponding to channel i with center frequency f_i. The transmission line resonators are coupled to the feedline and to power-detectors with independently adjustable coupling strengths, ie. capacitors, or in the specific example discussed here, proximity coupling between microstrip lines. The resonator frequencies are arranged monotonically and physically spaced at approximately $\lambda_i/4$ from neighboring channels. The response of an individual filter channel can be modeled as a dissipative shunt resonator, with a coupling-Q (Q_{feed}) to the feedline and a dissipative-Q (Q_{det}) associated with the power per cycle deposited in the detector. The resonator resolution is given by

$$\mathcal{R} = Q_r^{mm} = \Big(\frac{1}{Q_{\text{feed}}} + \frac{1}{Q_{\text{det}}}\Big)^{-1} = \frac{f_i}{\Delta f_i} \tag{1}$$

where f_i and Δf_i are the center frequency and width of channel i, and Q_r^{mm} is the total resonator Q. Maximum absorption occurs when $Q_{\text{feed}} = Q_{\text{det}}$. The full spectrometer is created by starting from the highest frequency channel f_u , then decreasing in frequency according to a geometric progression: f_u , $x\, f_u$, $x^2\, f_u$, . . . $x^{N_c-1}\, f_u$, where $x < 1$ is the frequency scaling factor, given by

$$x = \exp\Big(-\frac{\ln f_u - \ln f_l}{N_c - 1}\Big) \tag{2}$$

and N_c is the total number of channels. The ratio of the channel spacing to resolution is given by the oversampling factor Σ, where

$$N_c = \Sigma\mathcal{R}\ln(f_u/f_l). \tag{3}$$

As Σ increases, the total in-band absorption efficiency will become larger than 50%, the maximum value for an isolated single resonator. For an initial SuperSpec demonstration instrument with 600 channels with $\mathcal{R} = 700$ arranged from 195 to 310 GHz, $\Sigma = 1.85$ and the total in-band absorption efficiency is approximately 80%. (Neglecting losses in the feed line, etc.)

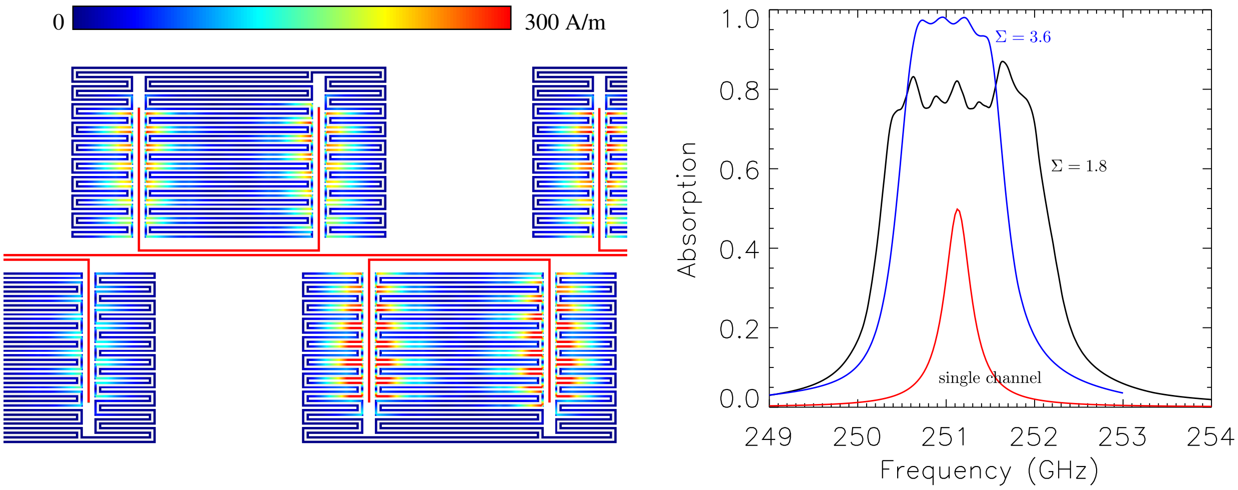

Figure 1. **(left)** A simulation showing the time-averaged magnitude of the current present in part of an 8-channel SuperSpec filter bank when driven at a specific frequency. mm-wavelength radiation incident from the left along the central microstrip feedline couple to U-shaped microstrip resonators, which in turn excite currents in the TiN meanders. **(right)** The total power absorbed for the 8-channel filter bank with two different oversampling factors, with the response of a single isolated channel shown for comparison.

Figure 1 shows the implementation of this concept for the SuperSpec prototype. The mm-wave circuit design summarized here and its coupling to a metal feedhorn are discussed in more detail in Barry et al.[6] In this design, the feedline and resonant filters are realized using inverted microstrip. This microstrip consists of superconducting Nb traces with a $1\,\mu$m width on Si substrate beneath a $0.5\,\mu$m thick amorphous silicon-nitride ($\mathrm{Si_3N}_x$) dielectric and a Nb ground plane. This feedline structure provides a $30\,\Omega$ characteristic impedance, suffers negligible radiation loss, allows for adequate proximity coupling between feedlines, and can be readily coupled to the lumped-element KID (LEKID) design discussed below without the need for vias or challenging step-coverage solutions.

The U-shaped half wave resonators are fabricated from the same Nb microstrip as the feedline. The center portion is proximity coupled to the feedline, while the tines couple to a lossy meander made from titanium nitride (TiN). Radiation at frequencies above the superconducting gap in the TiN film ($T_c \sim 2\,$K) breaks superconducting (Cooper) pairs and generates quasiparticles in the TiN LEKID inductive meander. This results in a perturbation of the complex impedance ($\delta\sigma(\omega) = \delta\sigma_1 - j\delta\sigma_2$) producing a measurable change in the dissipation and resonant frequency of the LEKID. The LEKID response is thus a direct measure of the power dissipated in the device. In the mm-wave circuit, the 20 nm thick TiN meander can be regarded a resistive $\sim 50\,\Omega/\square$ material.

Q_{feed} and Q_{det} can be adjusted by varying the length of the overlap region and the gaps separating the half wave resonator, the feedline, and the TiN meander. Starting with an estimate based on the analytic treatment of coupled microstrip lines in Abbosh et al.,[7] the final design for the prototype filter bank was based on simulations using Sonnet Software[*], a commercial, 3D planar, method-of-moments solver. Intended values of f_0, Q_{feed}, Q_{det} are interpolated on a grid of simulation results to obtain design values for l_0, G, and G_a, the resonator length, gap between the resonator and feed, and gap between the resonator and absorber, respectively. To allow for rapid simulation, infinitely-thin films are used in the model, and an additional correction is then included by hand to account for the improved coupling associated with finite film thickness based upon a sparse set of thick film simulations.

In practice, the the feed-resonator gap appropriate for our target $\mathcal{R} \sim 700$ channels is the most critical lithographic dimension, which has driven us to maximize the overlap region consistent with the $\lambda/4$ spacing of our highest frequency channels. The Deep-UV lithography stepper at the the Microdevices Laboratory (MDL) at

[*]http://www.sonnetsoftware.com

the Jet Propulsion Laboratory (JPL) can readily achieve line widths and feature spacing of $\sim 1 \pm 0.1\mu$m, which should allow for the construction of well matched filters with any value of $\mathcal{R}$ larger than approximately 200. For an $\mathcal{R} = 700$ absorber, variations in the Nb linewidth by $0.1\,\mu$m lead to a $\pm 8\%$ change in $\mathcal{R}$ and a negligible change in absorption efficiency. The thickness of the Si_3N_x dielectric is the most significant material parameter; the magnitude of this error approaches to our lithographic tolerances at the level of 3% total thickness variation. (The circuit is equally sensitive to the dielectric constant of this material, though we expect less wafer-to-wafer variation in this parameter.) The cumulative effect of less-critical tolerances, such as the TiN linewidth, mask alignment, and TiN thickness and resistivity lead to an additional and largely orthogonal 5% variation in $\mathcal{R}$.

3. KID DESIGN

The signal power admitted by each SuperSpec filter resonator is read out using a LEKID that consists of an inductive portion made from the TiN meander described previously and a interdigitated capacitor (IDC) made from the same material, as shown in figure 2. These KIDs make use of the novel properties of TiN films: high normal-state resistivity of $\sim 100\,\mu\Omega$-cm and thus a large kinetic inductance fraction, a variable critical temperature which can be adjusted by varying deposition conditions, and low losses suitable for making high-Q resonators. To estimate material properties for this design we use values from Leduc et. al.[8]

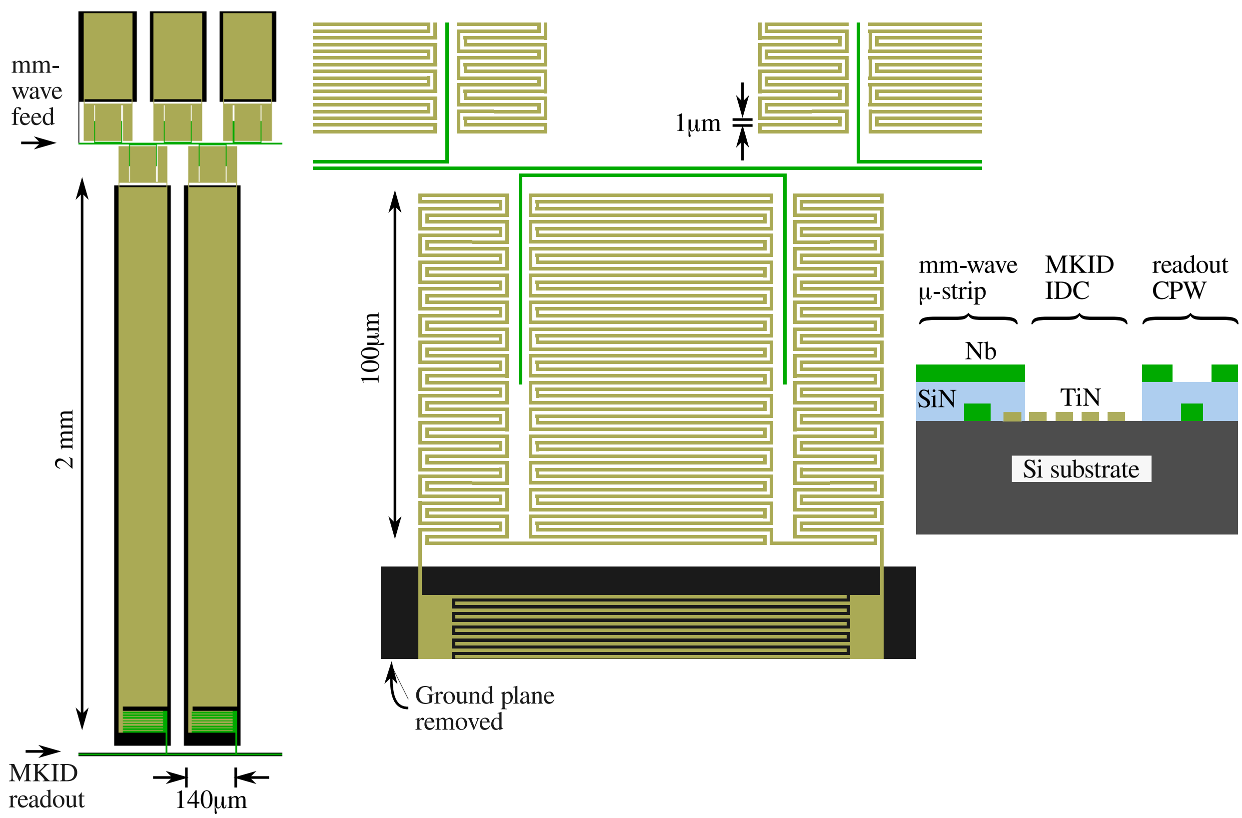

Figure 2. **(center)** The mm-wave portion of a single channel. Radiation from the left propagates along the green Nb microstrip line and excites the U-shaped half-wave resonator, which in turn couples to the amber TiN meander. The TiN meander forms the inductive portion of a KID, and is connected to a large IDC. **(left)** A wider view showing several nearby channels. Below the KID IDC, a second, smaller IDC couples the KID resonator to a readout line, made from bridged Nb CPW. In the region around the IDCs, shown in black, the ground plane and dielectric have been removed. **(right)** A cross-section showing the device layers in the region of the mm-wave circuit, the IDC, and the readout line. Not shown is a thin SiO_2 protective layer which is deposited between the TiN and the nitride and removed with an HF dip from the region around the IDC.

The design of the physical dimensions of the SuperSpec KIDs begins with a multiplexing density specification: we require the ability to multiplex one 600-channel spectrometer within a single octave of readout bandwidth. We can then determine a minimum required value for the resonator Q_r, where

$$\frac{\Delta f}{f} = \frac{1}{Q_r} = \frac{1}{Q_i} + \frac{1}{Q_c}, \tag{4}$$

and Q_i and Q_c are the internal and coupling Qs of the resonator. (Note that the resonators and Q values here all refer to the readout circuit operating at frequencies of a few hundred MHz, rather than the mm-wave filterbank circuit.)

The values of Q_r required to avoid unacceptable losses to collisions between resonators is then calculated using a Monte-Carlo simulation that assumes the following: the resonator targets are uniformly distributed in logarithmic frequency, each resonator at design frequency f_i scatters randomly by an amount δ_i described by a Gaussian probability distribution with $\sigma_f = \sqrt{< \delta_i/f_i >}$, and any two resonators whose shifted positions lie within five times the resonator bandwidth are lost. For plausible values of σ_f equal to 0.001 and 0.01, choosing $Q = 10^5$ results in the loss of 2.4%, and 3.6% of channels, respectively. These values approach the most optimistic expectations for fabrication yield, and suggest that we can comfortably choose $Q_r = 10^5$.

Although various resonator architectures can, in principle, produce devices with $Q_i > 10^5$ and sufficiently low two-level system (TLS) noise, we've chosen the conservative approach and use IDCs patterned on bare, crystal Si substrate; a resonator design which reliably produces high-Q resonators with relatively low TLS noise. To avoid the need for vias and complicated step-coverage, we have therefore chosen the inverted microstrip design for the mm-wave circuit discussed above, which allows the TiN layer deposition to occur as the first processing step. (See figure 2.)

By operating at a readout frequency of a few hundred MHz, we can significantly reduce the cost and complexity of readout hardware and also reduce the effect of TLS noise by increasing $\beta(\omega)$, the ratio of the frequency response to the dissipation response of a resonator, which scales as $\beta \propto kT/\omega$.[9] For the prototype device, we've chosen to use the $100 - 200$ MHz range. Future mutli-pixel implementations will likely cover several octaves of bandwidth.

With the required Q for multiplexing and readout frequency specified, the SuperSpec inductor is then designed to meet the following set of requirements. (1) T_c must be less than 2.6 K in order to absorb photons at the 190 GHz edge of our observation band. (2) The internal Q associated with dissipation loss due to optically generated quasiparticles must be compatible with the $Q \sim 10^5$ requirement from multiplexing considerations. (3) The inductor area should be largely contained with a few dissipation lengths of the region where mm-wave absorption occurs. (4) The operating temperature should be as high as possible, in order to minimize TLS noise, while still satisfying the requirement that the density of optically-generated quasiparticles should be significantly larger than the density of thermally generated quasiparticles. (5) The value of the inductance should be maximized, subject to the above constraints, in order to minimize die size.

Using the standard Mattis-Bardeen formulas for the complex conductivity of a superconductor (as summarized in Zmuidzinas et. al.[9]), and implementing the above conditions, we arrive at a design for the SuperSpec KID with physical dimensions and estimates of physical properties given in table 1. This design uses the thinnest TiN film which we expect to be able to deposit with high yield and well-controlled properties, with $T_c = 2K$ and an operating temperature of 250 mK appropriate for a He-sorption refrigerator.

The fundamental limit to the sensitivity of the SuperSpec design will be TLS noise. This source of excess noise was detected early in in the development of KIDs[10] and is now known to arise from fluctuations of the resonator capacitance due to the presence of microscopic TLS fluctuators in amorphous dielectrics.[11–14] The noise does not arise in the kinetic inductance detecting element itself, so it is possible to engineer the device to bring the TLS noise well below the fundamental photon noise. For SuperSpec, our approach is to bring the readout frequencies down from a few GHz to a few hundred MHz. This strategy can be understood by examining the condition on the spectral density of TLS fractional frequency noise S_{TLS} for achieving photon-noise limited operation,[9]

Table 1. Summary of the expected properties of the SuperSpec detectors for a demonstration instrument

Spectral res. (=mm-wave resonator quality factor) ($Q_r = R$)	700
Optical bandwidth per detector ($\delta\nu$)	$0.3 - 0.7$ GHz (e.g. 0.4)
Estimated system optical efficiency	0.25 - 0.5 $\times$ 1 pol
Photon occupation number at the detector (n)	0.5 - 5 (e.g. 1)
Optical power per detector (W)	0.5 - 3.0 $\times 10^{-}$13
Photon NEP at the detector (W Hz$^{-1/2}$)	2-4 $\times 10^{-18}$
Operating temperature ($T_{\rm op}$)	250 mK
TiN transition temp (T_c)	2 K
KID resonator quality factor	10^5
TiN film thickness (t) and line width (w)	10 nm, 1 μm
Inductor Volume	135μm^3
Quasiparticle recombination time (τ)	30 μs
Photo-produced quasiparticle number (N_{qp})	1-10 $\times 10^4$
Photo-produced quasiparticle density (n_{qp})	80-800 μm^{-3}
Thermal quasiparticle density (n_{qp}^{th})	≥ 4 μm^{-3}

$$S_{\rm TLS} < A\frac{\beta^2}{4Q_{\rm qp}^2}\frac{1+n_0}{n_0\delta\nu} \tag{5}$$

Here $n_0 \sim 1$ is the photon occupation number, $\delta\nu \sim 400$ MHz is the spectral resolution, $Q_{\rm qp}$ is the internal quality factor due to quasiparticle dissipation, A is a dimensionless factor of order unity, and β is the ratio between the frequency and dissipation response of the resonator discussed previously. For a readout frequency of 200 MHz and operating temperature of 250 mK, we have $\beta \approx 26$. We thus require $S_{\rm TLS} \lesssim 2 \times 10^{-17}{\rm Hz}^{-1}$. Recent measurements by our group indicate that for interdigitated capacitors on bare silicon, this should be a straightforward requirement to meet.[15]

Each KID is coupled to the readout feedline using a small interdigitated capacitor, one side of which is patterned in the TiN material while the other is patterned in the Nb feature layer. Because the coincidence of a short across the coupling capacitor *in addition* to a pinhole short to the ground plane in the inductor of a single KID would effectively disable the entire feedline circuit, we've chosen to use 2μm features and 2μm gaps for all of the coupling capacitor IDCs.

Since the inductor portion of the KID is beneath a dielectric layer and ground plane, the capacitance between the inductor and the ground plane dominates the current return-path to ground. For the dimensions shown here, we expect this capacitance, C_g, to be roughly 0.5 pF. So long as this value is small compared to the resonator capacitance, the loss mechanisms present in this parallel plate capacitor can be neglected. The coupling capacitor is chosen for a target value of Q_c, given by

$$Q_c = \frac{8C}{\omega_0 C_e^2 Z_0} \tag{6}$$

where the effective coupling capacitance, $C_e = (C_c\,C_g)/(C_c+C_g)$, approaches C_c in the case where $C \gg C_g \gg C_c$.

Each resonator is connected via its coupling capacitor to a 50 Ω coplanar waveguide (CPW) readout feedline. This feedline has a 7 μm wide center conductor made from the Nb feature layer, and a 4μm gap. The CPW ground plane is made from the top-layer Nb ground plane, and is continuous across most of the surface area of the chip. CPW ground straps, consisting of 5μm wide bridges of the ground plane over the top of the center conductor, with intact dielectric between the two, are placed approximately every 250 μm along the feedline. The input and output of the readout line consist of a tapered, fixed-impedance transition to wirebond pads that connect to a matching CPW line on the readout package.

To maximize the likelihood of achieving our target frequency spread, all of the inductors in the SuperSpec prototype are designed to have the same properties. The small differences in inductor length associated with the variable gap between the inductor and fixed-width tines is compensated by an adjustable length of vertical inductive line connecting the capacitor and the meander. To determine the appropriate capacitor for each KID resonator, a series of SONNET simulations are run on models KIDs spanning a range of discrete capacitor sizes, and the results were fit to a semi-analytic model which was then used to determine the capacitor length corresponding to a target frequency.

4. PROTOTYPE TEST DEVICE

The first SuperSpec test device consists of all of the mm-wave device and KID features; however, it does not include the horn-coupling hardware and cannot receive optical power. The same mask set should be compatible with future horn and waveguide-probe designs. The device consists of a $1.16\,\mathrm{cm}^2$ die fabricated on a stock 100 mm-diameter silicon wafer. The process includes 5 depositions (TiN, a protective SiO_2layer over the TiN, feature Nb, Si_3N_x dielectric, and Nb ground plane), and four lithographic steps, of which only two include critical μm-scale features and alignment. The final, horn-coupled design will be fabricated on a silicon-on-insulator (SOI) wafer with a 25μm device layer, and will include two additional deep reactive ion etch (DRIE) steps to define the probe and the die outline. A photograph of the prototype die is shown in figure 3.

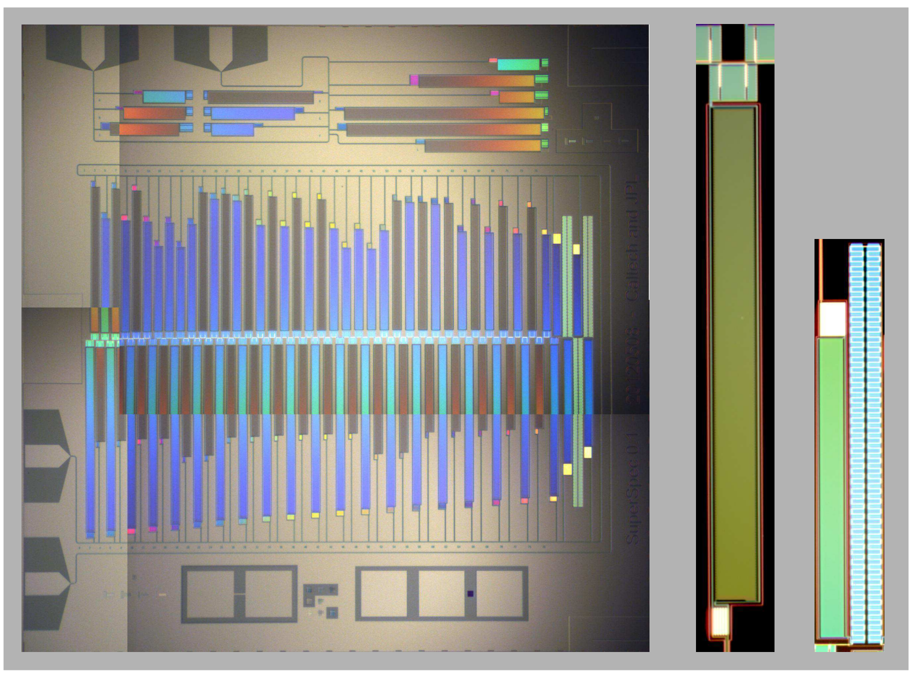

Figure 3. **(left)** A mosaic image made from several microscope photographs of the first SuperSpec prototype device. The die is a square with side length 1.08 cm. The (electrically disconnected) mm-wave feedline begins in the center left of the image and couples to the main row of mm-wave resonators and associated KIDs before reaching the terminating meander at the center right. The main readout line starts at the bottom left and connects to the coupling capacitor of each main line KID, then returns to a second pair of CPW bond pads at the bottom left. A second feedline couples to a sparse array of 12 test devices at the top of the image. Additional test structures for measuring resistivity and step coverage reliability are distributed along the bottom of the die. **(center)** An enlarged image showing a single KID resonator coupled to the mm-wave feedline. **(right)** An enlarged image of a portion of the termination meander.

The prototype device includes three types of mm-wave features: 74 tuned mm-wave filters, 3 in-line broadband detectors, and a terminating absorber. The 74 tuned filters span the $200-300$ GHz band. These include both isolated, individual filters and groups of five with a range of oversampling factors (Σ). Design values of Q_{det} and Q_{feed} independently sample the range from 600 to 2800, and include the demonstration instrument goal of

$2\mathcal{R} = 1400$. The in-line broad-band detectors consist of a short ($< \lambda_{\rm min}/4$) feedline meander in close proximity to a TiN absorber similar to that used in the tuned filters. Sonnet simulations predict roughly 0.5% absorption across the full optical band with a slowly varying frequency dependence for these test devices. The terminating absorber consists of several cm of meandered feedline surrounded by TiN meander with a 1 μm separation, and is designed to absorb any radiation which arrives at the end of the feed and reduce reflections to < 20dB. Four long segments of the terminating absorber are used as the inductors for an addition set of broad-band absorber KIDs. These are designed with readout frequencies well outside of the band of the typical KIDs in order to avoid frequency collisions arising from the imperfect simulation of inductors with different geometries.

The mm-wave frequencies of the main readout line devices are arranged in descending, monotonic order. The readout frequencies are arranged so as to minimize the potential for electromagnetic coupling between devices and to allow for the unambiguous identification of individual channels.[16] The band is broken into seven discrete sub-bands, as shown in figure 4, and neighboring pixels are drawn from different sub-bands such that each pixel is separated from its four nearest neighbors by at least 1/4 of the full readout bandwidth. The three smaller sub-bands all correspond to pixels with a the same design values of Q_r^{mm}, which will facilitate laboratory tests conducted with a broad-band optical source.

All the KIDs which surround the mm-wave line are connected to the same CPW readout feedline. In addition to this main readout line, the prototype device also includes a sparse array of 12 test resonators. These KIDs are similar to the standard design, but include a range of inductor sizes and both 1μm and 2μm IDCs, arranged so that each combination is repeated across a range of roughly 1.5 in readout frequency. The test devices also include a design variation in which the ground plane and dielectric is entirely removed from the area surrounding the inductor and an explicit parallel plate capacitor instead provides current return to ground.

5. INITIAL TEST RESULTS

Following fabrication, a group of seven dies were measured for room-temperature resistance and shorts to ground. All but one had similar values and closely matched expectations. One of these dies was then mounted in a light-tight sample box and tested cryogenically. The sample was connected to the cryostat input through a 40 dB cold attenuator, and the output connected to a cryogenic silicon-germanium amplifier with approximately 35 dB gain and then to the cryostat output ports. The stage was cooled with a dilution fridge to a base temperature of 20 mK. The device was then connected to a vector network analyzer (VNA) though an additional 90 dB of warm attenuation on the input and ~ 90 dB of warm amplification on the output. We see evidence of the onset of bifurcation at a readout power of approximately -130 dBm at the device input.

Device yield for this prototype chip appears promising: resonances were seen for 74 of the 77 typical KIDs on the main feedline. Three of the four expected low-frequency, termination KIDs were also seen, although it is likely the fourth landed below the 40 MHz cutoff frequency of the VNA. All of the measured devices appear to be lower in frequency than the design value by approximately 55%. The measured distribution of frequencies is reasonably fit by applying a single linear correction independently to all of the devices with 1 μm and 2 μm IDCs. Comparing the data to the corrected design values, we can confidently identify the individual channels and determine that the three missing devices are all have IDCs with 2μm features, as shown in figure 4.

At present, we have not yet determined the cause of the observed frequency shift, although we expect to resolve the matter easily. The most likely candidates are some combination of a smaller than expected TiN linewidth, a thinner than expected TiN layer, higher than expected TiN resistivity, or a lower than expected value of T_c. (Mattis-Bardeen theory predicts the last three terms modify the kinetic inductance as $L_s \propto R_s/\Delta$). A preliminary examination of the variation of resonator frequency with temperature suggests that T_c may be significantly lower than the design value, most likely just below 1 K. We are currently in the process of obtaining additional data to verify this.

Each resonance was measured at a fridge temperature of 20 mK, far below our expected operating temperature. Under these conditions, Q_c should remain unchanged, but Q_i will be determined by a combination of the residual quasiparticle density in the TiN and losses in the circuit. In this case, the dominant source of loss should be the lossy dielectric through which the KID inductor is weakly capacitivy coupled to the ground plane. After

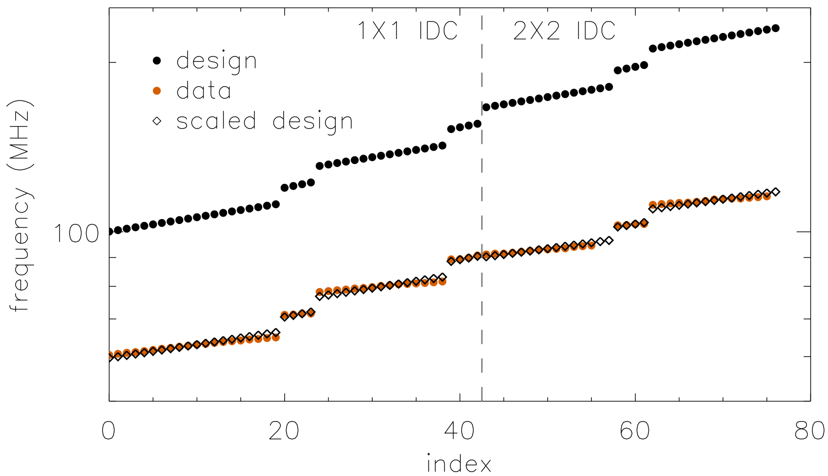

Figure 4. A comparison of the design frequencies and observed frequencies for the prototype devices. The vertical line separates the devices which have 1μm IDC features from those with 2μm IDC features. The design values (black dots) can be be roughly fit to the observed resonances (red dots) by applying a linear scaling (black diamonds).

corrections to account for amplifier gain variation and cable delay, a fit was performed to the complex resonator response, given by

$$S21(f) = a(1 - \frac{Q_r/Q_c e^{j\phi_0}}{1 + 2jQ_r((f - f_0)/f_0)}) \tag{7}$$

where a and ϕ_0 are an arbitrary amplitude and phase, f is the measured frequency, and f_0 is the resonant frequency.

A histogram of the fitted values of Q_c and Q_i are shown in figure 5. Measured values of $\log Q_c$ are tightly clustered, with a standard deviation of 0.06 dex. The mean value of $< Q_c >= 3.6 \times 10^5$ is higher than the design value; however, if we assume that the coupling capacitor value is correct and scale the design value to account for the frequency offset, we accurately predict the measured value. The large measured values of Q_i indicate that there are no unexpected loss mechanisms in the circuit, and that with an appropriate stage temperature and loading we should be able to reach our target value of Q_r.

Additional laboratory tests of the device described here are currently in progress, and we expect soon to report on both the fractional frequency noise and Q_i as a function of temperature, from which responsivity and (with some assumptions about coupling efficiency) an optical NET can be estimated.

6. CONCLUSION

We have presented the initial design of an ultra-compact spectrometer-on-a-chip for millimeter and submillimeter wavelength astronomy. Detailed simulations have been used to design a filter bank spectrometer consisting of planar, lithographed superconducting transmission line resonators coupled to KID detectors, and to verify the design is robust to realistic fabrication and design tolerances. Lumped-element, TiN KIDs have been designed which couple well to the mm-wave radiation, are optimized for the expected loading and stage temperature, and will accomodat the multiplexing of ~ 600 channels per octave at readout frequencies of hundreds of MHz.

An initial, dark prototype array consisting of 77 KIDs and additional test structures has been fabricated. Early results from the first cryogenic tests of this device show a very high yield, consistant resonator frequencies, tightly clustered coupling-Qs consistant with the design goals, and adequately high low-temperature dissipation-Qs. Testing of these devices is ongoing.

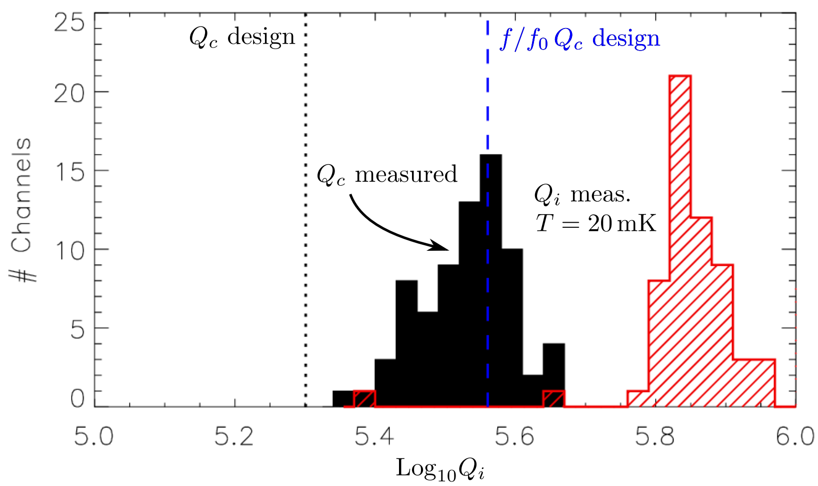

Figure 5. The black filled histogram shows the measured values of Q_c for the prototype device. Black dotted line is the target value of Q_c, which becomes the blue dashed line after scaling by observed resonator frequency. The red hashed histogram shows measured values of Q_i well below the design operating temperature.

Our collaboration has designed and fabricated a machined, metal feedhorn optimized for the lower SuperSpec band. A broad-band waveguide transition to the microstrip on our devices has been simulated and is currently being fabricated. The design of an optical prototype, which will be identical to the dark test device except for the addition of mm-wave probe features is in progress. In the coming year we expect to demonstrate a pair of observation-grade, 600 channel, $\mathcal{R} = 700$ spectrometer pixels, one operating in the 1-mm atmospheric window and the other covering the 650 and 850 micron bands. This instrument will serve as a pathfinder for future multi-pixels cameras, including a proposed CCAT instrument currently called *X-Spec*, which will consist of hundreds of SuperSpec pixels.

ACKNOWLEDGMENTS

This project is supported by NASA Astrophysics Research and Analysis (APRA) grant no. 399131.02.06.03.43. E. Shirokoff, C. McKenney, and L. J. Swenson acknowledge support from the W. M. Keck Institute for Space Studies. M. I. Hollister, L. J. Swenson, and T. Reck acknowledge support from the NASA Postdoctoral Programme. P. S. Barry acknowledges the continuing support from the Science and Technology Facilities Council Ph.D studentship programme and grant programmes ST/G002711/1 and ST/J001449/1. Device fabrication was performed the JPL Microdevices Laboratory.

REFERENCES

1. A. Kovács, P. Barry, C. Bradford, G. Chattopadhyay, P. Day, S. Doyle, S. Hailey-Dunsheath, M. Hollister, C. McKenney, H. LeDuc, *et al.*, "Superspec: design concept and circuit simulations," in *Proc. of SPIE Vol*, **8452**, pp. 84522G–1, 2012.
2. J. A. Tauber and N. R. Erickson, "A low-cost filterbank spectrometer for submm observations in radio astronomy," *Review of Scientific Instruments* **62**(5), pp. 1288–1292, 1991.
3. C. J. Galbraith, R. D. White, L. Cheng, K. Grosh, and G. M. Rebeiz, "Cochlea-based RF channelizing filters," *IEEE TRANSACTIONS ON CIRCUITS AND SYSTEMS I-REGULAR PAPERS* **55**, pp. 969–979, MAY 2008.
4. C. J. Galbraith, *Cochlea-Inspired Channelizing Filters for Wideband Radio Systems*. PhD thesis, U. Michigan, 2008.

5. A. Endo, P. Werf, R. M. J. Janssen, P. J. Visser, T. M. Klapwijk, J. J. A. Baselmans, L. Ferrari, A. M. Baryshev, and S. J. C. Yates, "Design of an Integrated Filterbank for DESHIMA: On-Chip Submillimeter Imaging Spectrograph Based on Superconducting Resonators," *Journal of Low Temperature Physics* **167**, pp. 341–346, May 2012.
6. P. Barry, E. Shirokoff, A. Kovács, T. Reck, S. Hailey-Dunsheath, C. McKenney, L. Swenson, M. Hollister, H. Leduc, S. Doyle, *et al.*, "Electromagnetic design for superspec: a lithographically-patterned millimetre-wave spectrograph," in *SPIE Astronomical Telescopes+ Instrumentation*, pp. 84522F–84522F, International Society for Optics and Photonics, 2012.
7. A. Abbosh, "Analytical closed-form solutions for different configurations of parallel-coupled microstrip lines," *"IET Microwaves, Antennas & Propagation"* **3**(1), pp. 137–147, 2009.
8. H. G. Leduc, B. Bumble, P. K. Day, B. H. Eom, J. Gao, S. Golwala, B. A. Mazin, S. McHugh, A. Merrill, D. C. Moore, O. Noroozian, A. D. Turner, and J. Zmuidzinas, "Titanium nitride films for ultrasensitive microresonator detectors," *Applied Physics Letters* **97**, p. 102509, Sept. 2010.
9. J. Zmuidzinas, "Superconducting microresonators: Physics and applications," *Annual Review of Condensed Matter Physics* **3**(1), pp. 169–214, 2012.
10. P. K. Day, H. G. LeDuc, B. A. Mazin, A. Vayonakis, and J. Zmuidzinas, "A broadband superconducting detector suitable for use in large arrays," *Nature* **425**, pp. 817–821, Oct. 2003.
11. J. Gao, J. Zmuidzinas, B. A. Mazin, H. G. Leduc, and P. K. Day, "Noise properties of superconducting coplanar waveguide microwave resonators," *Applied Physics Letters* **90**, p. 102507, Mar. 2007.
12. S. Kumar, J. Gao, J. Zmuidzinas, B. A. Mazin, H. G. Leduc, and P. K. Day, "Temperature dependence of the frequency and noise of superconducting coplanar waveguide resonators," *Applied Physics Letters* **92**, p. 123503, Mar. 2008.
13. J. Gao, M. Daal, J. M. Martinis, A. Vayonakis, J. Zmuidzinas, B. Sadoulet, B. A. Mazin, P. K. Day, and H. G. Leduc, "A semiempirical model for two-level system noise in superconducting microresonators," *Applied Physics Letters* **92**, p. 212504, May 2008.
14. O. Noroozian, J. Gao, J. Zmuidzinas, H. G. Leduc, and B. A. Mazin, "Two-level system noise reduction for Microwave Kinetic Inductance Detectors," in *American Institute of Physics Conference Series*, B. Young, B. Cabrera, and A. Miller, eds., *American Institute of Physics Conference Series* **1185**, pp. 148–151, Dec. 2009.
15. C. McKenney, H. Leduc, L. Swenson, P. Day, B. Eom, and J. Zmuidzinas, "Design considerations for a background limited 350 micron pixel array using lumped element superconducting microresonators," in *SPIE Astronomical Telescopes+ Instrumentation*, pp. 84520S–84520S, International Society for Optics and Photonics, 2012.
16. O. Noroozian, P. Day, B. H. Eom, H. Leduc, and J. Zmuidzinas, "Crosstalk reduction for superconducting microwave resonator arrays," *Microwave Theory and Techniques, IEEE Transactions on* **60**, pp. 1235 –1243, may 2012.

J Low Temp Phys
DOI 10.1007/s10909-014-1122-8

Design and Performance of SuperSpec: An On-Chip, KID-Based, mm-Wavelength Spectrometer

E. Shirokoff · P. S. Barry · C. M. Bradford · G. Chattopadhyay · P. Day · S. Doyle · S. Hailey-Dunsheath · M. I. Hollister · A. Kovács · H. G. Leduc · C. M. McKenney · P. Mauskopf · H. T. Nguyen · R. O'Brient · S. Padin · T. J. Reck · L. J. Swenson · C. E. Tucker · J. Zmuidzinas

Received: 10 September 2013 / Accepted: 28 January 2014

Abstract SuperSpec is an ultra-compact spectrometer-on-a-chip for mm and submm wavelength astronomy. Its very small size, wide spectral bandwidth, and highly multiplexed detector readout will enable construction of powerful multi-object spectrometers for observations of galaxies at high redshift. SuperSpec is a filter bank with planar, lithographed, superconducting transmission line resonator filters and lumped-element kinetic inductance detectors made from Titanium Nitride. We have built an 81 detector prototype that operates in the 195–310 GHz band. The prototype has a wide-band metal feed horn with a transition to microstrip that feeds the filter bank. The prototype has demonstrated optical filter bank channels with a range of resolving powers from 300 to 700, measured fractional frequency noise of $10^{-17}\mathrm{Hz}^{-1}$ at 1 Hz.

Keywords Kinetic inductance detectors · Resonators · Millimeter-wavelength · Spectroscopy

E. Shirokoff (✉) · S. Hailey-Dunsheath · M. I. Hollister · A. Kovács · C. M. McKenney · S. Padin · J. Zmuidzinas · R. O'Brient
California Institute of Technology, Pasadena, CA, USA
e-mail: erik.shirokoff@caltech.edu

P. S. Barry · S. Doyle · P. Mauskopf · C. E. Tucker
School of Physics and Astronomy, Cardiff University, Cardiff, Wales, UK

C. M. Bradford · P. Day · H. G. Leduc · H. T. Nguyen · T. J. Reck · L. J. Swenson · J. Zmuidzinas · G. Chattopadhyay · R. O'Brient
Jet Propulsion Laboratory, Pasadena, CA, USA

P. Mauskopf
Arizona State University, Tempe, AZ, USA

Published online: 14 February 2014

1 Introduction

SuperSpec is an ultra-compact, wide-band spectrometer-on-a-chip for mm and submm wavelength astronomy [1,2]. The kinetic inductance detector (KID)-based design outlined here and in the accompanying paper[1] is a specific example of the filter-bank spectrometer circuit discussed in Kovács et al. [3]. The basic design is similar to other filter-bank spectrometers which appear in the literature by Tauber and Erickson [4], Galbraith et al. [5], Galbraith [6] and the contemporary project DESHIMA [7,8]. The tomographic ionized-carbon mapping experiment (TIME) project is testing devices which use a similar microstrip filter bank coupled to transition edge sensor (TES) bolometers.[2]

In this design, mm-wave radiation propagates along a feedline and past a series of half-wavelength transmission line mm-wave resonators. Each resonator is coupled to the feedline and to a power-detector, and thus functions as a tuned filter. The resonator frequencies are arranged monotonically and physically spaced quarter-wavelength from neighboring channels to minimize interaction between resonators.

The response of an individual filter channel at frequency f_i can be modeled as a shunt resonator. Its resolving power is given by $\mathscr{R} = f_i/\Delta f_i = 1/Q_{\mathrm{feed}} + 1/Q_{\mathrm{det}} + 1/Q_{\mathrm{loss}}$, where the three Qs correspond to the coupling to the feedline, the power per cycle deposited in the detector, and the power per cycle which is absorbed elsewhere in the surrounding environment (e.g., $(\tan\delta)^{-1}$).

For efficient absorption, $Q_{\mathrm{feed}} = Q_{\mathrm{det}}$. The full spectrometer is created by arranging channels in a geometric progression, with a ratio of channel resolution to channel spacing determined by an adjustable oversampling factor Σ. As Σ increases, the total filter bank absorption efficiency can be larger than the 50 % maximum absorption in a single channel. A proposed 500 channel, $\mathscr{R} = 500$ SuperSpec demonstration instrument covering the 195–310 GHz band has $\Sigma = 2.1$ and greater than 80 % total absorption in band.

2 SuperSpec Prototype Design

The implementation of this filter bank design for the first generation SuperSpec prototype is shown in Fig. 1. The feedline and filter bank resonators are made from inverted microstrip consisting of 1 μm wide Nb traces on bare Si substrate, a 0.5 μm thick silicon nitride (Si_3N_x) dielectric deposited by plasma enhanced chemical vapor deposition and a Nb ground plane. The detectors are lumped-element KID (LEKIDs) made from 20 nm thick titanium nitride (TiN), with a transition temperature of approximately 2K [9,10]. The half-wavelength mm-wave resonator is proximity-coupled to both the feedline and to the meandered inductive portion of the KID. The coupling strengths can be independently tuned by adjusting the width of the gap between features.

The KID inductor is connected to an interdigitated capacitor (IDC) made from the same TiN layer deposited directly on the Si substrate. The ground plane and dielectric

1 Hailey-Dunsheath et al., JLTP, submitted.

2 Staniszewski et al., JLTP, submitted.

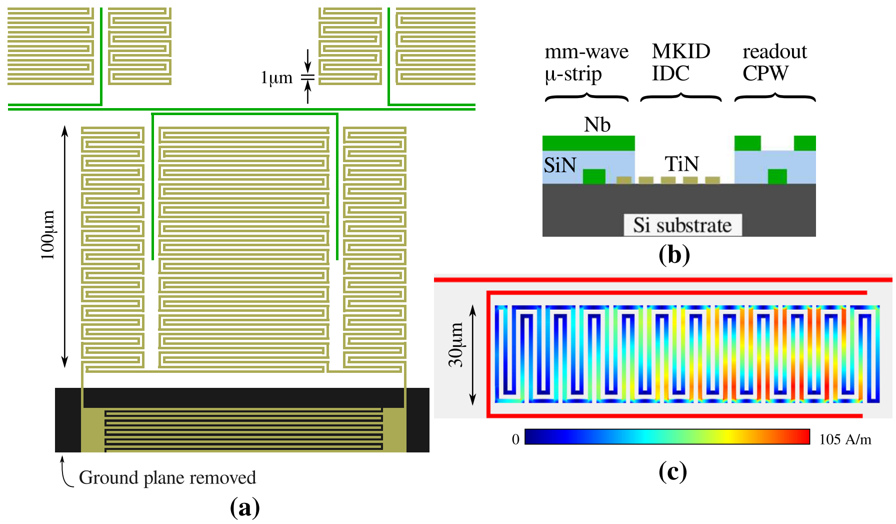

Fig. 1 **a** SuperSpec device detail, showing one full mm-wave resonator (*green* U-shaped structure), feedline, and the inductor and *top* portion of KID capacitor for one channel. **b** Cross section showing layers used in **a**. A thin SiO_2layer for etch selectivity between the TiN and SiN layer is not shown. **c** Simulation of the new design (see Sect. 4), showing time-averaged current distribution at a single optical frequency. *Solid-red* currents in Nb microstrip are off-scale (Color figure online)

layer are removed in the region surrounding the capacitor to minimize the presence of two-level systems (TLSs) in regions of high electric field. The microwave readout line consists of 50 Ohm, bridged Nb CPW. The 7 μm wide center conductor is made from same layer as the Nb microstrip features. A small IDC couples each KID to the feedline, and its value determines the KID coupling-Q. The capacitance between the KID inductor and the ground plane dominates the current return path, but makes a negligible contribution to dissipation and TLS noise.

Both the mm-wave circuit and KID resonator were designed using the commercial, 3D planar method-of-moments solver Sonnet. The finite thickness of the Nb film increases the coupling by 50 % compared to thin film values at these dimensions. Sonnet's multi-sheet thick metal model was used to correct for thickness effects, after verifying that such a models agreed with ANSYS HFSS simulations of simplified mm-wave resonators.

The first generation prototype die includes 73 filtered channels, arranged in a sparse array from 180–270 GHz. These are arranged in several five-channel filter-banks and many isolated channels, some with intentionally mismatched Q_{feed} and Q_{det} designed to test simulation results. In addition to the filtered channels, the prototype includes eight broad-band detectors, for a total of 81 KIDs. Four of these broad-band detectors are identical to the filtered detectors, except that they are proximity coupled directly to the feedline and spatially distributed among the filtered channels. The remaining four broad band detectors are incorporated into a terminator that consists of several centimeters of meandering feedline surrounded by closely spaced TiN.

Incident radiation couples to a multiple-flare-angle smooth-walled horn [11]. The circular waveguide output from the horn transitions into single mode oval waveguide

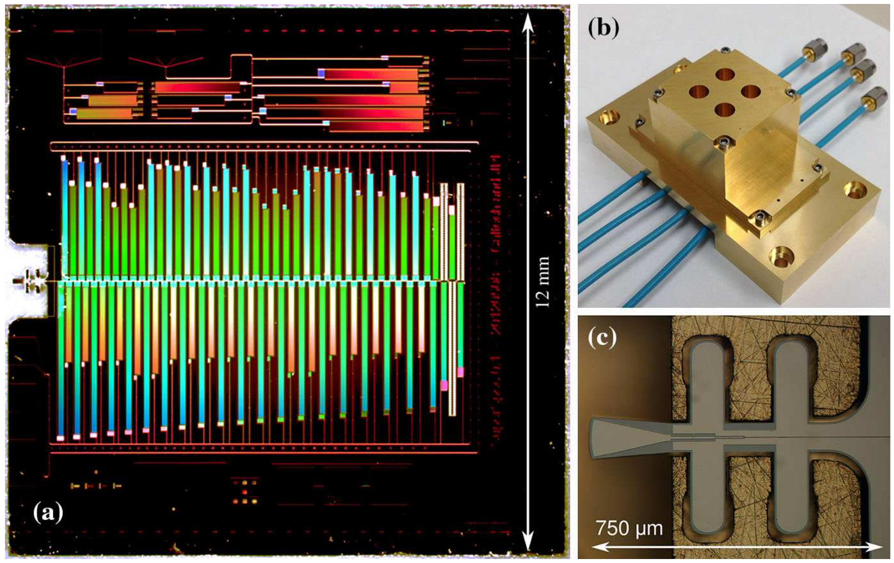

Fig. 2 **a** Prototype SuperSpec die; mm-wave feedline runs from *left* to *right* along the center past an array filter channels. A second array of dark test devices is located at the *top* of the die. **b** Four channel prototype horn block and test package. **c** Wide-bandwidth mm-wave probe mounted in the horn waveguide (Color figure online)

to couple to a waveguide probe fabricated on the 25 μm thick device layer of the SOI wafer which supports the spectrometer chip. The radial stub probe transitions through a CPW transmission line to form the broadband impedance match between the waveguide and the microstrip of the spectrometer. By careful design of the ground plane of the waveguide probe, coupling to higher order modes in the probe channel is suppressed without the need for wire bonds or beam-leads [12]. Simulation of this design show a coupling efficiency above 90 % from 190 to 310 GHz. A low pass capacitive metal-mesh filter is placed directly above horn to block harmonics.

3 Measured Performance

The prototype filter was tested in an optical cryostat cooled by a commercial pulse tube cooler (PTC) and a ^{3}He sorption refrigerator with a base temperature of 225 mK. The prototype horn block shown in Fig. 2 looks into the room through a 4K cold aperture, three metal-mesh low pass filters, a quartz IR blocker with low-density polyethylene (LDPE) anti-reflection coatings, and a 70 mm clear aperture high-density polyethylene (HDPE) window.

In cold tests of several devices from the most recent optical wafer, the median yield for operable KID resonators is 78 out of the 81 expected optical devices, with no critical flaws that disable an entire array. Values of the coupling quality factor (Q_c) are consistently close to the design value of 2×10^5, while the internal quality factor (Q_i) is $\geq 10^6$. The total quality factor, $Q_r = 1/(1/Q_i + 1/Q_c)$, is shown for a typical device in Fig. 3.

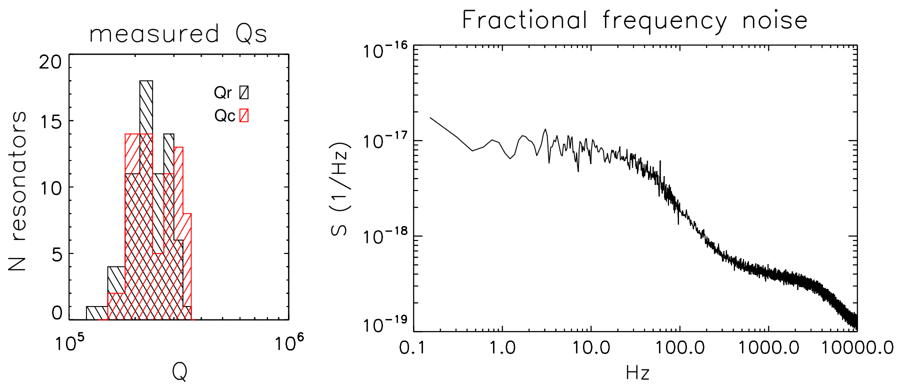

Fig. 3 (*Left*) measured readout Q values for one SuperSpec array. (*Right*) measured fractional frequency noise for a recent single SuperSpec detector under conditions specified in the text (Color figure online)

The responsivity of SuperSpec channels was inferred using beam-filling absorber placed outside the cryostat window at a temperature of either 300 or 77 K, in conjunction with the measured channel profiles. When Q_{loss} is small, the total optical power on an isolated, filter-coupled detector at frequency F_{mm} with matched mm-wave Qs will be approximately $P_{\mathrm{opt}} = \eta k \Delta T F_{\mathrm{mm}}/2\mathscr{R}$, where η includes an estimated 70 % transmission through the optical filter stack and 50 % power loss to beam truncation at 4 K inside the cryostat, and we have assumed a single-moded, single-polarization horn. For a detector with $R \sim 300$ and $F_{\mathrm{mm}} = 250$ we expect a 0.45 pW difference in loading.

The most responsive $\mathscr{R} \sim 300$ channels tested exhibit a fractional frequency shift of $\Delta F/F = 10^{-5}$, corresponding to an estimated responsivity-volume product $RV = 8 \times 10^{8} \mu\mathrm{m}^{3}\,\mathrm{W}^{-1}$, under a constant load of $7 \times 10^{-4}\,\mathrm{pW}\mu\mathrm{m}^{-3}$. These values do not include the effect of dissipating power in only a portion of the inductor volume, which increases the inferred response by at most a factor of two.

This inferred responsivity is much lower than predicted from Mattis-Bardeen relations, even assuming recently reported electron density of states, $N_0 = 4 \times 10^{10}\mathrm{eV}^{-1}\mu\mathrm{m}^{-3}$ [13,14]. It is also low compared to scaled measurements of the MAKO 350 μm camera pixels which are made from similar TiN films from the same facility [15]. We are currently investigating the source of this discrepancy. Significant problems with mm-wave coupling simulations seems unlikely for two reasons. First, measured $\mathscr{R}$ values of the widest filtered channels are close to design values. Second, the 10 dB drop in total power measured over the instrumented segment of the terminator agrees with simulations to within the uncertainty associated with our optical band.

Typical SuperSpec resonators from the most recent wafer show measured fractional frequency noise at the level of 1–$2 \times 10^{-17}\mathrm{Hz}^{-1}$ at a demodulated frequency of 1 Hz when operated 3 dB below bifurcation (−130 dBm at device input), at a stage temperature of 250 mK. A typical noise power spectral density (PSD) plot is shown in Fig. 3. The plateau at 1 kHz is first stage amplifier noise with an analog low-pass filter roll-off. The noise below 100 Hz is present only in the frequency direction of resonators. Readout power and temperature scaling suggest TLS noise is dominant, despite the shallower than $f^{-1/2}$ frequency dependence. More detailed characterization is currently underway.

4 Refined Second Generation Design

Using measured values for fractional frequency noise (S_{ffr}, the PSD in units of Hz^{-1}) and apparent responsivity (frequency shift in Hz/W) of the SuperSpec devices, we estimate an noise equivalent power (NEP) referenced at the detector of $\mathrm{NEP} = \sqrt{S_{\mathrm{ffr}}}/R = 3 \times 10^{-16}\,\mathrm{WHz}^{-1/2}$. This is significantly higher than the background limit for proposed science applications, and is due primarily to the low measured responsivity. We are currently pursuing two programs designed to improve this NEP.

The first is a systematic exploration of possible contributions to the low inferred responsivity, including independent checks on the horn and mm-wave probe transmission and the responsivity of TiN direct absorption camera pixels to radiation in our observing band. The second is a test chip redesign which includes both new diagnostic features and devices which have been modified to improve responsivity, decrease TLS noise, and increase resilience to fabrication variation (see Fig. 1c). The first test dies with the new design are in fabrication.

Acknowledgments This project is supported by NASA Astrophysics Research and Analysis (APRA) Grant No. 399131.02.06.03.43. ES, CMM, and LJS acknowledge support from the W. M. Keck Institute for Space Studies. MIH, LJS, and TR acknowledge support from the NASA Postdoctoral Program. PSB acknowledges the continuing support from the Science and Technology Facilities Council Ph.D. studentship programme and grant programmes ST/G002711/1 and ST/J001449/1. Device fabrication was performed the JPL Microdevices Laboratory.

References

1. E. Shirokoff et al., Proc. SPIE **8452**, 84520R (2012)
2. P.S. Barry et al., Proc. SPIE **8452**, 84522F (2012)
3. A. Kovács et al., Proc. SPIE **8452**, 84522G (2012)
4. J.A. Tauber, N.R. Erickson, Rev. Sci. Inst. **62**, 1288 (1991)
5. C.J. Galbraith et al., IEEE Trans. Circ. Syst. I **55**, 969 (2008)
6. C.J. Galbraith, Ph.D. thesis, U. Michigan (2008)
7. A. Endo et al., J. Low Temp. Phys. **167**, 341 (2012)
8. A. Endo et al., Appl. Phys. Lett. **103**, 032601 (2013)
9. H.G. Leduc et al., Appl. Phys. Lett. **97**, 102509 (2010)
10. S. Doyle et al., JLTP **151**, 530 (2008)
11. J. Leech et al., A&A **532**, A61 (2011)
12. J.W. Kooi et al., in *Fourteenth International Symposium on Space Terahertz Technology*, ed. by C. Walker, J. Payne, 2003, p. 127
13. J. Zmuidzinas, Ann. Rev. Cond. Matter Phys. **3**, 169 (2012)
14. J. Gao et al., Appl. Phys. Lett. **101**, 142602 (2012)
15. C.M. McKenney et al., Proc. SPIE **8452**, 84520R (2012)

J Low Temp Phys
DOI 10.1007/s10909-013-1068-2

Optical Measurements of SuperSpec: A Millimeter-Wave On-Chip Spectrometer

S. Hailey-Dunsheath · P. S. Barry · C. M. Bradford · G. Chattopadhyay · P. Day · S. Doyle · M. Hollister · A. Kovacs · H. G. LeDuc · N. Llombart · P. Mauskopf · C. McKenney · R. Monroe · H. T. Nguyen · R. O'Brient · S. Padin · T. Reck · E. Shirokoff · L. Swenson · C. E. Tucker · J. Zmuidzinas

Received: 6 September 2013 / Accepted: 23 December 2013

Abstract SuperSpec is a novel on-chip spectrometer we are developing for (sub)millimeter wavelength astronomy. Our approach utilizes a filterbank of moderate resolution ($R \sim 500$) channels, coupled to lumped element kinetic inductance detectors (KIDs), all integrated onto a single silicon chip. The channels are half-wave resonators formed by lithographically depositing segments of superconducting transmission line, and the KIDs are titanium nitride resonators. Here we present optical measurements of a first generation prototype, operating in the 180–280 GHz frequency range. We have used a coherent source to measure the spectral profiles of 17 channels, which achieve linewidths corresponding to quality factors as high as $Q_{\rm filt} = 700$, consistent with

S. Hailey-Dunsheath (✉) · M. Hollister · A. Kovacs · C. McKenney · R. O'Brient · S. Padin · E. Shirokoff · L. Swenson · J. Zmuidzinas
California Institute of Technology, Mail Code 301-17, 1200 E. California Blvd., Pasadena, CA 91125, USA
e-mail: haileyds@caltech.edu

P. S. Barry · S. Doyle · C. E. Tucker
School of Physics & Astronomy, Cardiff University, 5 The Parade, Cardiff CF24 3AA, UK

C. M. Bradford · G. Chattopadhyay · P. Day · H. G. LeDuc · R. Monroe · H. T. Nguyen · T. Reck
Jet Propulsion Laboratory, 4800 Oak Grove Drive, Pasadena, CA 91109, USA

A. Kovacs
Institute for Astrophysics, University of Minnesota, 116 Church St SE, Minneapolis, MN 55455, USA

N. Llombart
Optics Department of the Complutense University of Madrid, C. Arcos de Jalon No. 118, 28037 Madrid, Spain

P. Mauskopf
Arizona State University, 650 E. Tyler Mall, Tempe, AZ 85287, USA

Published online: 23 January 2014

the designed values plus additional dissipation characterized by $Q_i \approx 1440$. We have also used a Fourier Transform Spectrometer to characterize the spectral purity of all 72 channels on the chip, and measure typical out of band responses ∼30 dB below the peak response.

Keywords Kinetic inductance detector · Millimeter-wave · Spectroscopy

1 Introduction

The epoch of reionization and the birth and subsequent growth of galaxies in the first half of the Universe's history ($z \gtrsim 1$) are key topics in modern astrophysics. Measurements of the cosmic far-IR background indicate that in aggregate, much if not most of the energy released by stars and accreting black holes over cosmic time has been absorbed and reradiated by dust [3]. A complete understanding of galaxy evolution since reionization therefore requires observations at (sub)millimeter wavelengths, where the dust emission peaks, and the extinction of diagnostic spectral lines is minimized. Survey spectroscopy at (sub)millimeter wavelengths, using a multi-beam spectrometer such as we describe here, is uniquely poised to access the high-redshift Universe, both through the measurement of individual galaxies, and via statistical studies in wide-field tomography. In particular, the 158 μm [CII] transition is typically the brightest spectral feature in dusty galaxies, and promises to be a powerful probe of galaxies at redshifts $z \geq 3$, where it is shifted into the telluric windows at $\lambda \geq 600$ μm [7].

SuperSpec is a novel, ultra-compact spectrometer-on-a-chip for (sub)millimeter wavelength astronomy. Its very small size, wide spectral bandwidth, and highly multiplexed detector readout will enable construction of powerful multi-beam spectrometers for high-redshift observations. We are currently developing this technology with $R \sim 500$ spectrometers covering the 190–310 GHz band, with the aim of deploying a future wide-band survey spectrometer for the 25 m CCAT telescope, with tens of thousands of detectors employed in tens of beams covering the 190–520 GHz band. The proposed instrument will be optimized for measuring the bright atomic fine-structure and molecular rotational lines from interstellar gas in galaxies, and particularly for [CII] observations at $z \approx 3$–9. This same technology will also be deployed in the proposed TIME, a statistical survey instrument designed to tomographically map out the [CII] line during reionization (see Stanizewski proceedings).

2 First Generation Prototype

Free space radiation is coupled into a transmission line (the feedline) on our prototype chips using a direct-drilled, multiple-flare angle feed horn [1]. The circular waveguide output of the horn is converted to a single mode oval waveguide and fed with a planar probe, fabricated from the 25 μm thick device layer of a SOI wafer that forms the spectrometer chip (T. Reck, in prep). The probe couples through a CPW transition segment to the impedance-matched microstrip that forms the feedline. Simulations of this design show a coupling efficiency above 90 % from 190 to 310 GHz.

SuperSpec employs a filterbank architecture [4,1,6]. Incoming radiation propagates down the feedline past a series of tuned resonant filters, each of which consists of a section of transmission line of length $\lambda_i/2$, where λ_i is the resonant wavelength of channel i. These half-wave resonators are coupled to the feedline and to power detectors with adjustable coupling strengths (described by quality factors $Q_{\rm feed}$ and $Q_{\rm det}$, respectively) that determine the net filter quality factor $Q_{\rm filt}$, which is equal to the spectrometer resolving power R. The transmission line for both the feedline and the resonator is microstrip, consisting of superconducting Nb traces on a Si substrate beneath an amorphous silicon-nitride (Si_3N_x) dielectric and Nb ground plane. The signal power admitted by each resonator is dissipated in a segment of lossy meander formed from titanium nitride (TiN). Radiation at frequencies above the superconducting gap in the TiN film ($f \sim 147$ GHz for $T_c \sim 2$ K) breaks Cooper pairs and generates quasiparticles, resulting in a perturbation of the complex impedance.

The TiN meander is connected in parallel to an interdigitated capacitor (IDC) made from the same TiN material to form a lumped element kinetic inductance detector (KID) [6]. Perturbations to the complex impedance of the meander translate into changes in the dissipation and resonant frequency of the KIDs, which operate with resonant frequencies in the 100–200 MHz range. Each KID is coupled to a coplanar waveguide readout feedline (CPW) by a small coupling capacitor, formed by TiN on the KID side, and Nb on the readout side. The chip is cooled by a ^{3}He sorption refrigerator to 220 mK, which is sufficiently below the TiN T_c to keep the thermal quasipartical density below that of the optically-generated quasiparticles, while also as high as possible to minimize two-level system (TLS) noise.

We have fabricated and characterized a first generation prototype SuperSpec test device. This device includes three types of mm-wave features: 73 tuned mm-wave filters, 4 in-line broad-band detectors interspersed over the full length of the feedline, and a terminating absorber. The 73 tuned filters span the 180–280 GHz range, and have design values of $Q_{\rm feed}$ and $Q_{\rm det}$ targeting (with no additional dissipation) $Q_{\rm filt,design} =$ 300–1400. This range of $Q_{\rm filt,design}$ is intended to test our ability to tune the channel quality factor in the vicinity of $R \sim 500$. The in-line broad-band detectors consist of a short ($<\lambda_{\rm min}/4$) feedline meander in close proximity to a TiN absorber similar to that used in the tuned filters. The proximity coupling between the feedline and the absorber is designed for an approximately flat 0.5 % absorption across the full mm band, which produces an optical loading comparable to that in the spectrometer channels. The terminating absorber consists of a length of meandered feedline surrounded by TiN meander, and is designed to absorb any power arriving at the end of the feed (reducing reflections to $<$20 dB). Four long segments of the terminating absorber are used as the inductors for an additional set of broad-band absorber KIDs.

2.1 Coherent Source Measurements

We have characterized a subset of our channels using a local oscillator (LO) chain, which provides a $\times 15$ frequency multiplication of a microwave tone. The LO is coupled to a feed horn, and radiates directly into the cryostat. The source can be tuned to cover the 180–280 GHz range, and frequency sweeps across our band are used to measure the line profiles of individual channels. For the measurements presented here

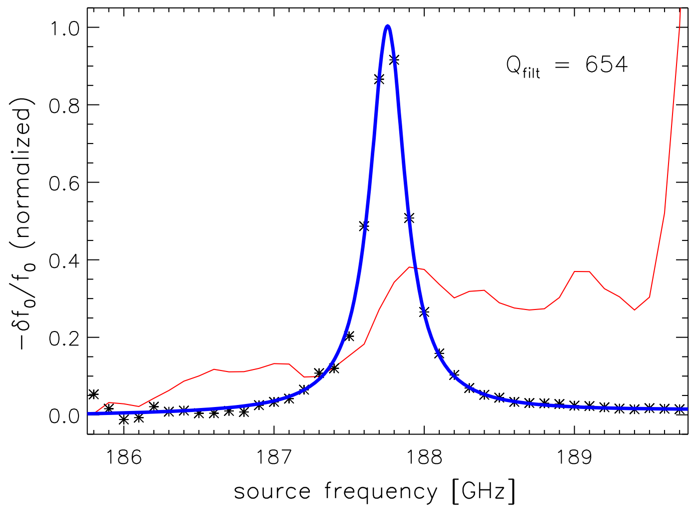

Fig. 1 Spectral profile of a high-Q ($Q_{\mathrm{filt}} = 654$) channel measured with a swept coherent source (*black points*) and a Lorentzian fit (*thick blue line*). Data points show the measured response normalized by the response of a broad-band KID (*thin red line*) (Color figure online)

we place a low-pass optical filter with cutoff at 210 GHz in the beam, in order to reject contamination from harmonics in the LO chain. This setup allows characterization of the 17 lowest frequency channels, with $f_0 = 184$–210 GHz, and $Q_{\mathrm{filt,design}} = 300$–$1400$. We note that two low-pass optical filters at 300 and 330 GHz inside the cryostat prevent excitation of the harmonics of the spectrometer resonators. The LO source is amplitude-modulated at 2 Hz, fast enough to avoid any excess low-frequency system noise. The KID is read out using a standard homodyne detection scheme, and we toggle the readout between a channel and a nearby broadband in-line KID used to normalize the channel response.

In Fig. 1 we show the peak-normalized profile of a representative high-Q channel. The fractional frequency response $\delta x = \delta f_0/f_0$ of the KID normalized by the peak value is:

$$\frac{-\delta x(f)}{(-\delta x)_{\mathrm{max}}} = \frac{1}{1 + 4Q_{\mathrm{filt}}^2\left(\frac{f-f_0}{f_0}\right)^2}, \tag{1}$$

where f_0 is the resonant frequency, and Q_{filt} is the filter quality factor. The filter quality factor is given by:

$$1/Q_{\mathrm{filt}} = 1/Q_{\mathrm{det}} + 1/Q_{\mathrm{feed}} + 1/Q_i, \tag{2}$$

where Q_{i} is the internal quality factor accounting for dissipative loss in the resonator [1]. In general, the line profiles are well characterized by Eq. 1, and fitting to this function allows an estimate of Q_{filt} for each channel. We measure filter quality factors as high as $Q_{\mathrm{filt}} = 700$, and this provides a conservative lower limit on the dissipative quality factor Q_i. An improved estimate of Q_i may be obtained by comparing

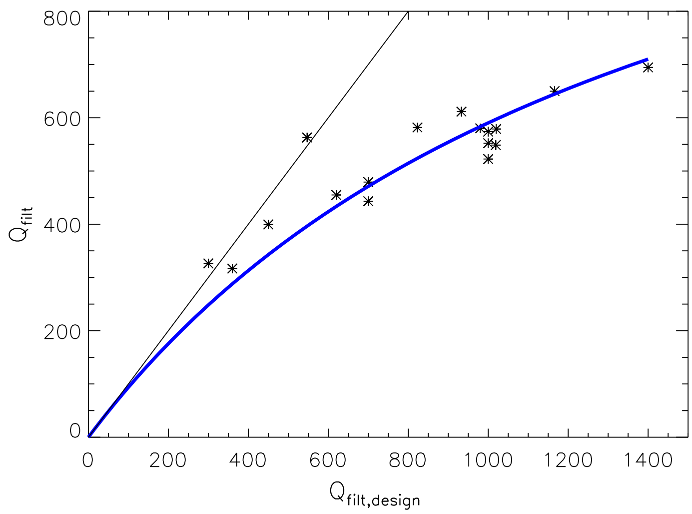

Fig. 2 Comparison of the measured and designed linewidths for the 17 channels at $f_0 = 184$–210 GHz and $Q_{filt,design} = 300$–1400 (see text). Some of the points with $Q_{filt,design} = 1000$ have a small horizontal offset for clarity. *Thin black line* is drawn for $Q_{filt} = Q_{filt,design}$, *thick blue line* shows $Q_{filt}^{-1} = Q_{filt,design}^{-1} + Q_i^{-1}$ for $Q_i = 1440$ (Color figure online)

the measured $Q_{\rm filt}$ with the designed loss-less quality factor, assuming the targeted values of $Q_{\rm det}$ and $Q_{\rm feed}$. This assumption is supported by the fact that we achieve the designed quality factor for $Q_{\rm filt} < 400$, where dissipative loss is negligible (Fig. 2). A fit to the set of all measured channels using Eq. 2 yields a best fit value of $Q_i = 1440$ (Fig. 2).

The dominant source of dissipation in the resonator is expected to be the silicon-nitride dielectric layer in the microstrip. The loss tangent inferred from our estimated Q_i is $\tan\delta = 1/Q_i = 7 \times 10^{-4}$. This value falls between published measurements of silicon–nitride at $f = 6$ GHz ($\tan\delta \approx 10^{-4}$) [5] and $f \approx 1.5$ THz ($\tan\delta \approx 5 \times 10^{-3}$) [2]. To operate efficiently as an astronomical spectrometer the dissipative losses must be sufficiently small to allow high detection efficiency with moderate resolving power. For a matched resonator ($Q_{\rm feed} = Q_{\rm det}$) the fraction of power on the feedline terminating in the detector on resonance is:

$$\eta_{\rm filt} = \frac{1}{2}\left[1 - \frac{Q_{\rm filt}}{Q_i}\right]^2. \qquad (3)$$

With no losses the filter efficiency is $\eta_{\rm filt} = 50$ %, and with $Q_{\rm i} = 1440$ this drops by less than a factor of 2 for $Q_{\rm filt} \leq 420$.

2.2 Fourier Transform Spectroscopy

We have obtained full band spectra for all channels using a Martin–Puplett Interferometer, with 293 and 78 K blackbodies at the input ports. The 73 spectrometer

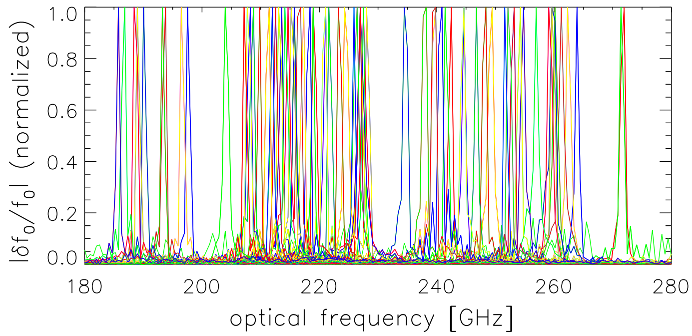

Fig. 3 Full set of 72 channel profiles, measured simultaneously with an FTS and CASPER-ROACH based FPGA multitone readout. Each color is a separate channel. Non-uniform sampling of frequency space is in part by design, and also reflects scatter between designed and measured f_0. Noise from 272 GHz channel produces features at 0.05–0.1 (*green*) (Color figure online)

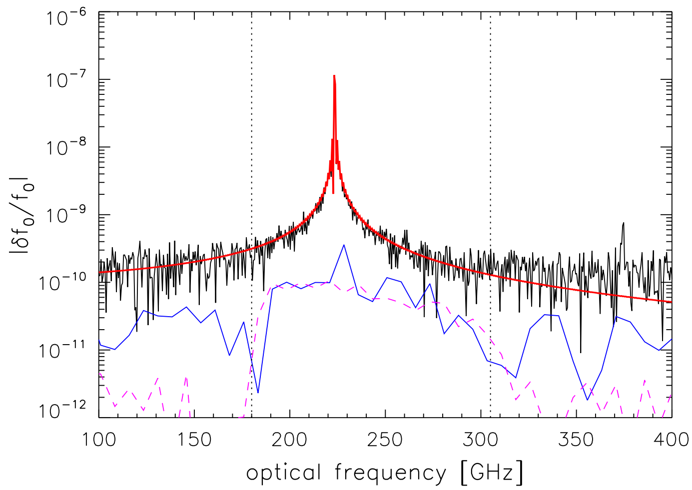

Fig. 4 FTS measurement of the spectral profile of a typical channel (*thin black*). Overplotted are a Lorentzian profile fit (*thin red*), the residuals binned (*thin blue*), the scaled profile of the first terminator (*dashed magenta*), and the expected bandpass defined by feed horn, waveguide probe, and metal-mesh filters (*dotted black vertical lines*). Outside of the narrow channel profile, the response is ∼0.1 % the peak value for most channels, and closely matches the profile measured on the terminator (Color figure online)

channels and 8 broadband KIDS were read out in parallel using a CASPER-ROACH based FPGA readout system. The fourier transform spectrometer (FTS) provides an unapodized spectral resolution of ≈0.6 GHz, compared with the 0.3–0.9 GHz width of the spectrometer channels. Compared with the LO measurements, the FTS measurements do not cleanly resolve the channel profiles, but they do provide a smooth spectral signal that better enables a characterization of the broad-band channel response. In Fig. 3 we show the normalized spectra of all functioning (72/73) channels.

In Fig. 4 we show the response of a representative channel, along with that of the first terminator. We fit models directly to the interferograms, and in general find that all channel profiles are well described by narrow Lorentzians. The residuals show a detectable broad-band response with the same spectral profile as that of the terminators and inline broad-band KIDs. This indicates a finite amount of direct coupling between the feed line and the channel KIDs that bypasses the half-wave resonators. For typical channels the broad-band response is $\sim 0.1\,\%$ of the peak in-band response.

Acknowledgments This project is supported by NASA Astrophysics Research and Analysis (APRA) Grant No. 399131.02.06.03.43. ES, CMM, and LJS acknowledge support from the W. M. Keck Institute for Space Studies. MIH, LJS, and TR acknowledge support from the NASA Postdoctoral Program. PSB acknowledges the continuing support from the Science and Technology Facilities Council Ph.D studentship programme and grant programmes ST/G002711/1 and ST/J001449/1. Device fabrication was performed the JPL Microdevices Laboratory.

References

1. P.S. Barry et al., in *Society of Photo-Optical Instrumentation Engineers (SPIE) Conference Series*, vol. 8452 (SPIE, Bellingham, WA, 2012)
2. G. Cataldo, J.A. Beall, H.-M. Cho, B. McAndrew, M.D. Niemack, E.J. Wollack, Opt. Lett. **37**, 4200 (2012)
3. D.J. Fixsen, E. Dwek, J.C. Mather, C.L. Bennett, R.A. Shafer, ApJ **508**, 123 (1998)
4. A. Kovács et al., in *Society of Photo-Optical Instrumentation Engineers (SPIE) Conference Series*, vol. 8452 (SPIE, Bellingham, WA, 2012)
5. A.D. O'Connell et al., Appl. Phys. Lett. **92**, 112903 (2008)
6. E. Shirokoff et al., in *Society of Photo-Optical Instrumentation Engineers (SPIE) Conference Series*, vol. 8452 (SPIE, Bellingham, WA, 2012)
7. R. Wang et al., ApJ **773**, 44 (2013)